Biomedical Optics EXPRESS

Automated analysis of investigational near-infrared fluorescence lymphatic imaging in humans

Jingdan Zhang,[1] Shaohua Kevin Zhou,[1,4] Xiaoyan Xiang,[1] Merrick L. Bautista,[2] Blake A. Niccum,[2] Gabriel S. Dickinson,[2] I-Chih Tan,[2] Wenyaw Chan,[3] Eva M. Sevick-Muraca,[2] and John C. Rasmussen,[2,*]

[1]*Whole Body and Oncology Image Analytics Program, Siemens Corporate Research, 755 College Road East, Princeton, New Jersey, 08540, USA*

[2]*Center for Molecular Imaging, The Brown Foundation Institute of Molecular Medicine, The University of Texas Health Science Center at Houston, 1825 Pressler Street, Houston, Texas, 77030, USA*

[3]*Division of Biostatistics, School of Public Health, The University of Texas Health Science Center at Houston, 1200 Herman Pressler St., Houston, Texas, 77030, USA*

[4]*Shaohua.Zhou@siemens.com (algorithm)*

** John.Rasmussen@uth.tmc.edu*

Abstract: ALFIA (Automated Lymphatic Function Imaging Analysis), an algorithm providing quantitative analysis of investigational near-infrared fluorescence lymphatic images, is described. Images from nine human subjects were analyzed for apparent lymphatic propagation velocities and propulsion periods using manual analysis and ALFIA. While lymphatic propulsion was more easily detected using ALFIA than with manual analysis, statistical analyses indicate no significant difference in the apparent lymphatic velocities although ALFIA tended to calculate longer propulsion periods. With the base ALFIA algorithms validated, further automation can now proceed to provide a clinically relevant analytic tool for quantitatively assessing lymphatic function in humans.

OCIS codes: (110.2960) Image analysis; (170.0110) Imaging systems; (170.2655) Functional monitoring and imaging; (170.3880) Medical and biological imaging.

References and links

1. S. D. Shpilfoygel, R. A. Close, D. J. Valentino, and G. R. Duckwiler, "X-ray videodensitometric methods for blood flow and velocity measurement: a critical review of literature," Med. Phys. **27**(9), 2008–2023 (2000).
2. T. Der, P. Bercik, G. Donnelly, T. Jackson, I. Berezin, S. M. Collins, and J. D. Huizinga, "Interstitial cells of cajal and inflammation-induced motor dysfunction in the mouse small intestine," Gastroenterology **119**(6), 1590–1599 (2000).
3. S. Kwon and E. M. Sevick-Muraca, "Non-invasive, dynamic imaging of murine intestinal motility," Neurogastroenterol. Motil. **23**(9), 881–e344 (2011).
4. K. Alitalo, T. Tammela, and T. V. Petrova, "Lymphangiogenesis in development and human disease," Nature **438**(7070), 946–953 (2005).
5. B. D. Lawenda, T. E. Mondry, and P. A. S. Johnstone, "Lymphedema: a primer on the identification and management of a chronic condition in oncologic treatment," CA Cancer J. Clin. **59**(1), 8–24 (2009).
6. S. A. Norman, A. R. Localio, S. L. Potashnik, H. A. Simoes Torpey, M. J. Kallan, A. L. Weber, L. T. Miller, A. Demichele, and L. J. Solin, "Lymphedema in breast cancer survivors: incidence, degree, time course, treatment, and symptoms," J. Clin. Oncol. **27**(3), 390–397 (2008).
7. J. C. Rasmussen, I. C. Tan, M. V. Marshall, K. E. Adams, S. Kwon, C. E. Fife, E. A. Maus, L. A. Smith, K. R. Covington, and E. M. Sevick-Muraca, "Human lymphatic architecture and dynamic transport imaged using near-infrared fluorescence," Transl Oncol **3**(6), 362–372 (2010).
8. I. C. Tan, E. A. Maus, J. C. Rasmussen, M. V. Marshall, K. E. Adams, C. E. Fife, L. A. Smith, W. Chan, and E. M. Sevick-Muraca, "Assessment of lymphatic contractile function after manual lymphatic drainage using near-infrared fluorescence imaging," Arch. Phys. Med. Rehabil. **92**(5), 756–764, e1 (2011).
9. K. E. Adams, J. C. Rasmussen, C. Darne, I. C. Tan, M. B. Aldrich, M. V. Marshall, C. E. Fife, E. A. Maus, L. A. Smith, R. Guilloid, S. Hoy, and E. M. Sevick-Muraca, "Direct evidence of lymphatic function improvement after advanced pneumatic compression device treatment of lymphedema," Biomed. Opt. Express **1**(1), 114–125 (2010).
10. H. W. Lim and N. A. Soter, *Clinical Photomedicine* (Marcel Dekker, 1993).

#169247 - $15.00 USD Received 24 May 2012; accepted 10 Jun 2012; published 22 Jun 2012

11. K. E. Adams, S. Ke, S. Kwon, F. Liang, Z. Fan, Y. Lu, K. Hirschi, M. E. Mawad, M. A. Barry, and E. M. Sevick-Muraca, "Comparison of visible and near-infrared wavelength-excitable fluorescent dyes for molecular imaging of cancer," J. Biomed. Opt. **12**(2), 024017 (2007).
12. E. M. Sevick-Muraca and J. C. Rasmussen, "Molecular imaging with optics: primer and case for near-infrared fluorescence techniques in personalized medicine," J. Biomed. Opt. **13**(4), 041303 (2008).
13. R. Sharma, W. Wang, J. C. Rasmussen, A. Joshi, J. P. Houston, K. E. Adams, A. Cameron, S. Ke, S. Kwon, M. E. Mawad, and E. M. Sevick-Muraca, "Quantitative imaging of lymph function," Am. J. Physiol. Heart Circ. Physiol. **292**(6), H3109–H3118 (2007).
14. S. Kwon and E. M. Sevick-Muraca, "Noninvasive quantitative imaging of lymph function in mice," Lymphat. Res. Biol. **5**(4), 219–232 (2007).
15. J. C. Rasmussen, I. C. Tan, M. V. Marshall, C. E. Fife, and E. M. Sevick-Muraca, "Lymphatic imaging in humans with near-infrared fluorescence," Curr. Opin. Biotechnol. **20**(1), 74–82 (2009).
16. A. Yilmaz, O. Javed, and M. Shah, "Object tracking: a survey," ACM Comput. Surv. **38**(4), 13–es, es (2006).
17. R. Bellman and S. E. Dreyfus, *Applied Dynamic Programming* (Princeton University Press, 1962).
18. R. H. Bartels, J. C. Beatty, and B. A. Barsky, *An introduction to splines for use in computer graphics and geometric modeling* (Morgan Kaufmann Publishers Inc, 1987).
19. G. Hellström, W. Fischer-Colbrie, N. G. Wahlgren, and T. Jogestrand, "Carotid artery blood flow and middle cerebral artery blood flow velocity during physical exercise," J. Appl. Physiol. **81**(1), 413–418 (1996).

1. Introduction

Movement of iodinated x-ray contrast agents within blood vessels and gastrointestinal tracts can define vessel lumens and, from dynamic imaging, can enable algorithmic estimation of blood flow and velocity [1] and gut motility [2] for disease diagnosis or surgical guidance. Image analysis algorithms for quantifying blood flow vary in complexity from simply determining the bolus transit time between two fixed regions of interest (ROIs) to iteratively solving the inverse mass transport problem to obtain volumetric flow rates [1]. However, because the velocity of arterial blood flow is directly impacted by its pulsatile nature, stenosis, vessel architecture, catheterization, and even injection of the contrast medium itself, no single algorithm is generally applicable, and other imaging technologies such as Doppler ultrasonography have largely supplanted efforts to assess blood flow rates with fluoroscopy. Imaging of x-ray contrast density has also been used to quantify motility in the gastrointestinal tracts of small animals using fluoroscopy [2] and more recently using fluorescent intensity and near-infrared fluorescence (NIRF) imaging [3]. In each case, spatiotemporal maps of the contrast density or intensity have enabled the quantification of the velocities of propagating peristaltic waves by determining the transit time of changing radiodensities or fluorescent intensities between two fixed regions of interest (ROIs).

Another important physiologic system in which peristaltic flow occurs is the lymphatic system, a poorly understood, unidirectional circulatory system that takes up excessive interstitial fluid and macromolecules and propels the acellular fluid (or lymph) through a network of capillaries, vessels, trunks, and lymph nodes to the blood circulatory system. For a more complete review of lymphatic architecture and function see Alitalo *et al.* [4].

The lymphatics play a critical role in fluid homeostasis. The most extreme condition of lymphatic failure manifests itself in the chronic disease of lymphedema, which is characterized by swelling, tissue fibrosis, and impaired immune response. The most common cause of lymphedema in the United States is lymphatic trauma incurred in the arms and legs of 3-5 million cancer survivors [5]. Cancer related lymphedema arises months to years after lymph node dissection, and/or radiation therapy [6]. There is no cure for lymphedema and for the past eighty years, standard of care treatment has largely been limited to complete decongestive therapy (CDT), a regimen of compression bandaging and manual lymphatic drainage (MLD), a gentle therapeutic massage designed to stimulate lymphatic propulsion. Yet there is no accepted quantitative standard-of-care imaging approach to assess lymphatic contractile propulsion, thereby limiting (i) diagnosis of dysfunctional lymphatics, (ii) selection of the most efficacious choice of lymphedema therapies, and (iii) development of new pharmaceutical agents to stimulate lymphatic function and ameliorate lymphedema.

Recently we developed NIRF lymphatic imaging to visualize the contractile propulsion of boluses of indocyanine green (ICG)-laden lymph within the lymphatics to quantify the contractile functional parameters of apparent propagation velocity and propulsion period in

#169247 - $15.00 USD Received 24 May 2012; accepted 10 Jun 2012; published 22 Jun 2012

normal control subjects [7], and in subjects with lymphedema before and after treatment with MLD [8], and with pneumatic compression devices [9]. While the approach to quantify lymphatic contractile function is similar to that used previously in fluoroscopy applications [1, 2], the manual nature of the analysis is time and user intensive, impeding real-time, quantitative lymphatic imaging. Herein we present the basis of a new algorithmic approach called Automated Lymphatic Function Imaging Analysis (ALFIA), which when completed will provide quantitative analysis of NIRF lymphatic images and facilitate translation of quantitative lymphatic imaging into the clinic. In this contribution, we describe the base algorithms of ALFIA, demonstrate its use to quantitatively analyze NIRF lymphatic images of nine human subjects, and validate the values of apparent lymphatic propagation velocities and propulsion periods against those independently obtained by manual evaluation of the images.

2. Methods

2.1 NIRF imaging

Near-infrared (NIR) light provides several advantages for imaging as compared to the visible band including (i) a minimal absorbance spectra of skin [10] enabling the propagation of photons deep within the tissue and (ii) low autofluorescence responsible for a significantly reduced noise floor [11]. In addition, repeated fluorophore excitation generates multiple fluorescence emission events per second enabling, with proper optical filter selection, sub-second image exposure times with high signal-to-noise ratios [12]. However, NIR photons are multiply scattered within tissues, potentially preventing the resolution of deep (> 3-4 cm) lymphatic structures without tomographic approaches. Still, in humans, the propulsion of lymph in superficial lymphatic vessels and nodes can be readily visualized following intradermal administration of micrograms of ICG as illustrated in Fig. 1 and Media 1. With rapid image acquisition, sequences of NIRF images have been shown to enable movies of lymphatic contractile function non-invasively in swine [13], mice [14], and humans [7, 15].

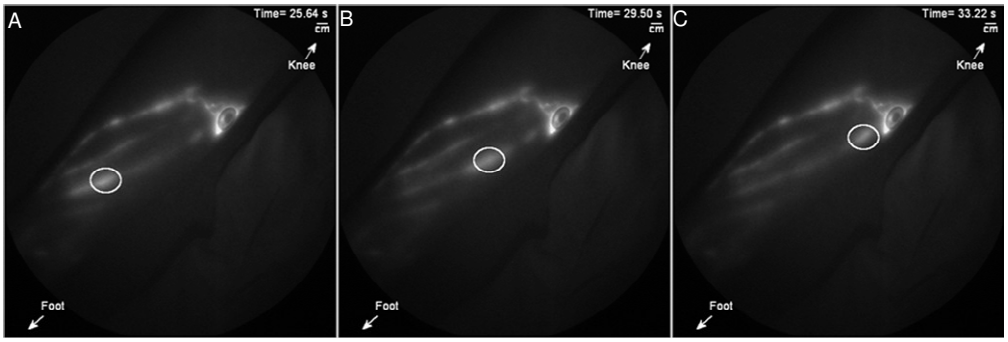

Fig. 1. Series of images illustrating the propagation of a bolus of fluorescent lymph (identified by ellipse) through a lymphatic vessel in the right shin of a 43 year old female (subject 8). The round shape near the right edge of the calf is a band-aid which covers an injection site at that location. These images are frames taken from Media 1 available online.

2.2 Clinical imaging

As part of a US Food and Drug Administration (IND# 102,765) and University of Texas Health Science Center at Houston institutional review board approved clinical study, three control subjects and six unilateral leg lymphedema subjects were recruited for NIRF imaging of leg lymphatics. After informed consent, each subject received multiple intradermal injections of ICG in both legs. Each injection was comprised of 25 µg ICG in 0.1 mL saline with a total dose ≤ 400 µg, which is below the approved intravenous dose of 2 mg/kg. Immediately following administration, subjects were imaged for approximately 2.5 hours, primarily in a supine position. Vital signs were monitored during imaging and a 24 hour

#169247 - $15.00 USD Received 24 May 2012; accepted 10 Jun 2012; published 22 Jun 2012

follow-up telephone call was made to monitor for adverse events. No adverse events were reported.

After intradermal injection of ICG, images of the fluorescent lymphatics in both legs were obtained using two custom NIRF imagers described previously [7]. Briefly, as illustrated in Fig. 2, each leg was illuminated by the diffused output of a 500 mW, 785 nm laser diode with a maximum tissue-surface incident power density <1.9 mW/cm^2. The non-ionizing laser light propagated up to several cm into the tissue and excited the transiting ICG in the superficial lymphatics. The resultant fluorescent signal was filtered using a 785 nm holographic notch filter and an 830 nm band-pass filter and focused onto the photocathode of a Gen III image intensifier. The intensified image was acquired using a custom, 16 bit, frame-transfer charge coupled device (CCD) camera and the images were saved onto a computer. The integration time on the CCD camera was 200 ms and, given the image readout times required, a total acquisition time was ~650 ms per image. Near real-time imaging of lymphatic propulsion was achieved and subjects were able to view their lymphatic function on a wall-mounted display. The NIRF images were independently analyzed manually and with ALFIA.

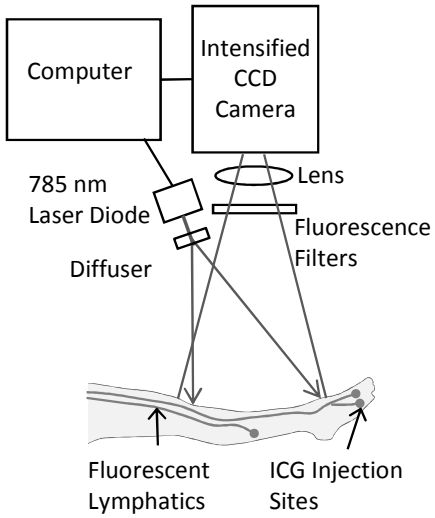

Fig. 2. Basic schematic of the near-infrared fluorescence imaging system.

2.3 Manual analysis

The manual analysis of NIRF lymphatic images was conducted as described elsewhere [7]. Briefly, as illustrated in Fig. 3, ROIs are selected along the lymphatic vessel and their average fluorescent intensities are plotted as a function of time. The apparent propagation velocity (v) of lymphatic propulsion is calculated by taking the ratio of the apparent distance (d) between two fixed ROIs and the transit time (Δt) for a bolus of lymph to propagate from one ROI to the other as shown in Eq. (1). As NIRF lymphatic imaging is a planar imaging technique, the distance is designated as "apparent" to reflect the lack of length information in the vertical dimension. In addition, the propulsion period, or time delay, between successive lymphatic propulsion events is determined. This approach to quantify lymphatic contractile function is similar to that used previously in fluoroscopy applications [1, 2], and the manual nature of the analysis is time and user intensive, impeding real-time, quantitative lymphatic imaging.

#169247 - $15.00 USD Received 24 May 2012; accepted 10 Jun 2012; published 22 Jun 2012

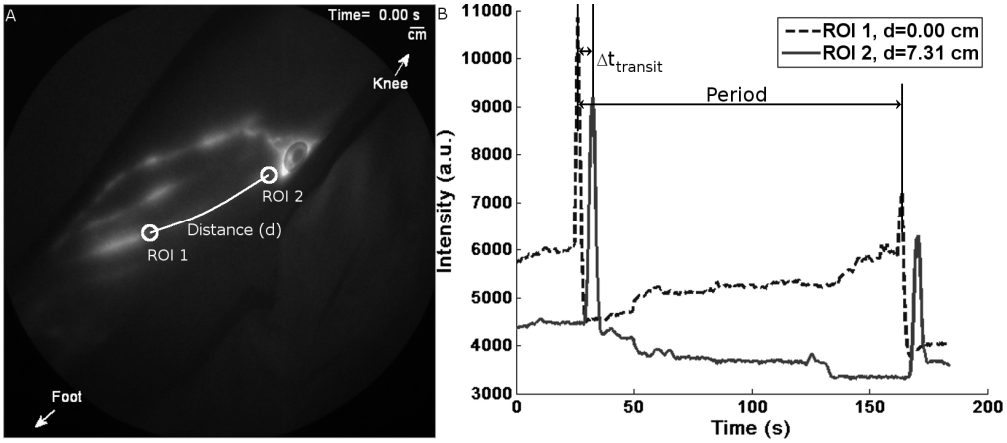

Fig. 3. Quantification of the lymphatic contractile functional parameters, apparent lymphatic propagation velocity and propulsion period. (A) Two regions of interest are selected on lymphatic vessel and the distance between the two is determined. (B) The fluorescent intensity profiles are then plotted and the transit time calculated as the time between the maximum intensities of the peaks corresponding to the same bolus of lymph. The propulsion period is the time between successive propulsion events in the same ROI.

$$v = \frac{d_{ROI2} - d_{ROI1}}{\Delta t} \tag{1}$$

Additionally, while lymphatic contractile function has been quantitated in small feasibility studies [7, 8, 15] it remains challenging due to (i) unknown vessel geometries depicted largely from the trajectory of a propelled bolus of fluorescent lymph, and (ii) the non-uniform fluorescent intensity along the lymphatic vessel. As shown in Fig. 4, large fluctuations in the fluorescent intensity also result from subject movement, changes in lymphatic vessel depth, and branching lymphatic architectures further limiting quantification of lymphatic contractile function to manual definition of vessel lumens from fluorescent trajectories and computation of propagation velocity from length of fluorescent bolus travel over a defined period of time.

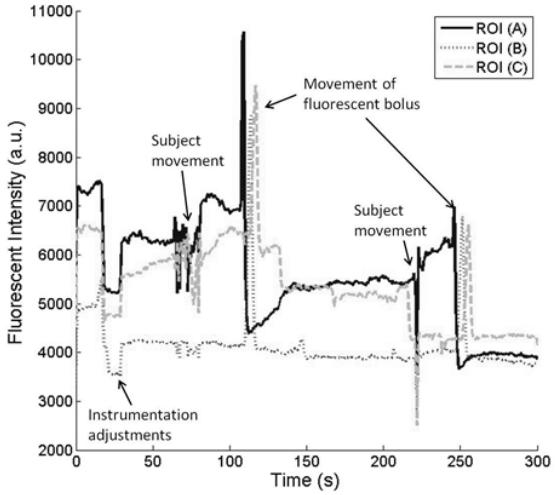

Fig. 4. Plots illustrating the impact of the propagation of boluses of fluorescent lymph, adjustment of instrumentation settings, and subject movement, on the fluorescent intensity profile of three regions of interest (ROIs). The ROIs correspond to the ellipses in Fig. 1 while the start time in Media 1 corresponds to ~83s on this plot.

#169247 - $15.00 USD Received 24 May 2012; accepted 10 Jun 2012; published 22 Jun 2012

2.3 ALFIA

While ALFIA uses the same basic methodology as described above to compute the lymphatic propagation velocity and propulsion period, several additional image analysis techniques were developed to reduce motion artifacts and to minimize the subject dependent errors. These techniques include an object tracking algorithm to stabilize the subject within the images and to reduce motion artifacts, an image representation named "flow map" to describe the propagation of fluorescence in the lymphatics more reliably, and a refinement algorithm to adjust the positions of flow lines identified by a user. The workflow of ALFIA is shown in Fig. 5(A) and described below.

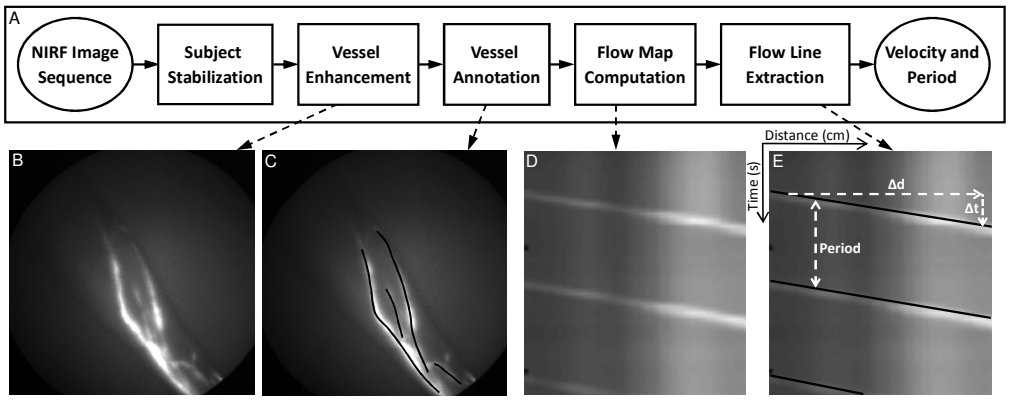

Fig. 5. (A) Analysis workflow of ALFIA. (B) An aggregated image is generated to facilitate vessel identification. (C) The lymphatic vessels are manually identified and annotated. (D) A flow map of fluorescent intensity as a function of distance (d) and time (t) is generated and (E) the flow lines of lymph propagation are manually annotated and automatically adjusted to select the maximal intensity value near the ends. The velocity (Δd/Δt) and propulsion periods are then calculated and exported to a spreadsheet.

2.3.1 Subject stabilization

After importing a sequence of NIRF images, the subject's movement is tracked and the images are transformed to reduce motion artifacts as follows. Given an image sequence, $\{I_1, I_2, I_3,\ldots, I_J\}$, we let the reference frame be I_1 and the transformation of the subject in I_1 to the subject in the jth frame I_j be T_j. As subject movements are typically small, the transformation is modeled as a 2D rigid translation. A large number of tracking algorithms for 2D rigid translation have been proposed in literature [16]. Herein we estimate T_j based on image appearance consistency and the smoothness constraint of the subject movement.

The stabilization algorithm first identifies a sparse set of salient points, $C_1 = \{c_1, c_2, c_3,\ldots, c_K\}$, belonging to the subject and/or a fluorescent lymphatic vessel in the reference frame I_1. In a NIRF image, the relative high intensity regions belong to the foreground subject, as the high fluorescent intensity value is caused by either a bolus of fluorescent lymph or lymphatic vessels stained by the NIR fluorophore. Following this observation, we sparsely sample the salient points from these high intensity regions. Then a set of image patches $Q_1 = \{q(I_1, c_1), q(I_1, c_2),\ldots, q(I_1, c_K)\}$ centered at the salient points are used to represent the image appearance of the subject at the reference frame I_1. The patch size needs to be carefully determined. On one hand, it needs to be big enough to include enough local subject appearance and be much larger (3-4 times) than the bolus of lymph to prevent lymph propagation from interfering with subject motion estimation. On the other hand, it cannot be too big to include too much background. In our experiments, the bolus width is generally 10-15 pixels and we empirically set the patch width to 40 pixels for 512x512 images. For jth frame with subject transformation T_j, the location of these salient points $C_j = \{T_j(c_1), T_j(c_2),\ldots, T_j(c_K)\}$ and the corresponding image patch set is $Q_j = \{q(I_j, T_j(c_1)), q(I_j, T_j(c_2)),\ldots, q(I_j, T_j(c_K))\}$.

#169247 - $15.00 USD Received 24 May 2012; accepted 10 Jun 2012; published 22 Jun 2012

For tracking, T_j is estimated by minimizing the energy function,

$$E\left(\{T_j\}\right)=\alpha\sum_{j=2}^{J}E_I\left(Q_1,Q_j\right)+\beta\sum_{j=2}^{J}E_I\left(Q_{j-1},Q_j\right)+\sum_{j=2}^{J}E_s\left(T_{j-1},T_j\right), \qquad (2)$$

where E_I measures intensity consistency of the subject between two images, $E_s(T_{j-1}, T_j)$ is the smoothness constraint between two consecutive frames, and $\alpha>0$ and $\beta>0$ are weight coefficients. Figure 6 shows a set of sampled salient points and explains Eq. (2).

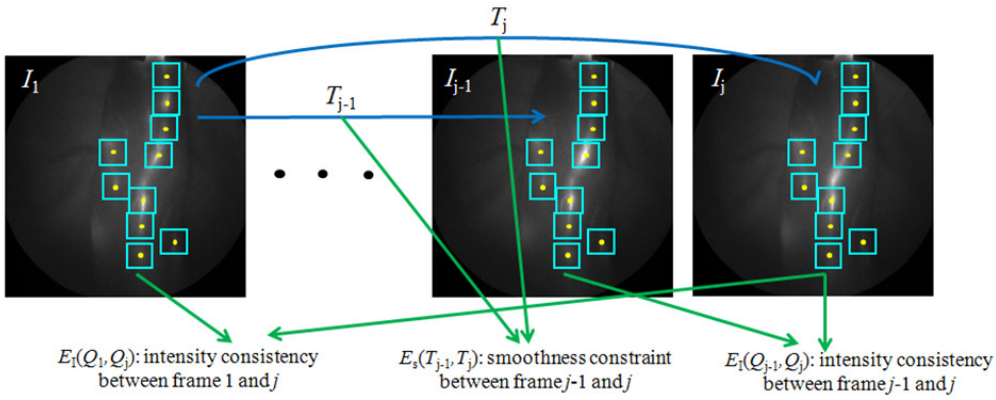

Fig. 6. Salient points (yellow dots) are sampled from the reference frame I_1. A set of image patches (cyan boxes) centered at the salient points are used to represent the image appearance of the subject. Transformation T_j, $j = 2, \ldots, J$, is estimated by minimizing Eq. (2), which encodes the intensity consistency constraints and the translation smoothness constraint.

The possibility of drifting is reduced by enforcing the intensity consistency between the reference frame and the tracking frames and between two consecutive frames. In our experiment, the term E_I is computed as the sum of the negative Normalized Cross-Correlation of each corresponding image patch, the term E_s is computed as Euclidean distance between two translations, and the choices of weight coefficients α and β are empirically decided. The total energy function E (Eq. (2) is minimized using Dynamic Programming [17].

2.3.2 Vessel enhancement and annotation

After subject stabilization, the vessel enhancement module computes an aggregated image to better visualize the lymphatic vessels. Often the entire lymphatic vessel structure cannot be clearly identified in one image, as at times only the parts of the vessels through which fluorescent boluses of lymph are actively transiting are visible in the images. The aggregated image is created by computing the maximum intensity of each pixel across the whole image sequence. The lymphatic architecture can be identified more reliably in the aggregated image. At this stage of development, the vessels are then annotated manually by the user. A spline [18] is used to represent a vessel and the user only needs to annotate several control points along its length.

2.3.3 Flow map computation

For each annotated vessel, points on the vessel are densely sampled. A flow map, M, of fluorescent intensity at these points across the sequence is computed. The flow map, a 2D intensity function of position on the vessel and time, is computed to capture the movement of fluorescence in the vessel. $M(n, j)$ represents the intensity of the nth sample point at the jth frame. It is computed as

$$M\left(n,j\right)=\frac{1}{\left|N\left(u_n,v_n\right)\right|}\sum_{(u,v)\in N(u_n,v_n)}I_j\left(u,v\right), \qquad (3)$$

#169247 - $15.00 USD Received 24 May 2012; accepted 10 Jun 2012; published 22 Jun 2012

where (u_n, v_n) is the image coordinate of the nth point; $N(u_n,v_n)$ defines a small neighborhood around (u_n,v_n); $|N(u_n,v_n)|$ is the number of pixels within $N(u_n,v_n)$; and I_j is the intensity map of the jth frame. The computation is illustrated in Fig. 7. Figure 5(D) shows the flow map computed from the longest vessel in Fig. 5(C).

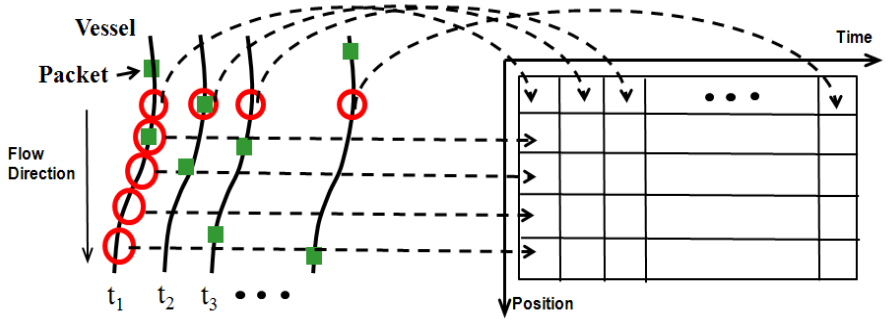

Fig. 7. Flow map computation on a vessel. The value of a pixel in the flow map is computed by averaging the intensity of a small region (circles) on a specific position of the vessel and in a specific image frame. If the region includes a lymph bolus (square), the value of the pixel will be higher. The x axis is the time (t_j) that the images were acquired and the y axis is the position or distance of each region from the first region selected on the vessel.

2.3.4 Flow line extraction

In the flow map, M, the movement of fluorescent lymph along the lymphatic vessel is depicted by straight, sloped lines called flow lines as seen in Fig. 5(D). Because the intensity profile of some flow lines are too weak to be detected reliably by automatic line detection algorithms currently available, the flow lines are identified manually. The position of each identified flow line is optimized automatically by exhaustively searching for the local line with the highest intensity profile. An example of extracted lines is shown in Fig. 5(E). Finally, the apparent propagation velocity and the propulsion period are estimated by computing the slope (Δdistance/Δtime) of each flow line and the time interval between two consecutive flow lines respectively. The results are exported to a spreadsheet.

2.4 Statistical analysis

Repeated measurement ANOVA (linear mixed model) was used to compare the apparent propagation velocities and propulsion periods of the lymphatic function between those calculated from AFLIA and the manual analysis. Common correlation is assumed for any two measurements of the dependent variable recorded from the same subject. Because the data was analyzed with both programs independently, the vessel selection varied between each program, resulting in data sets which were not always pairable and incomplete pairs were included in the analysis to increase the precision of the estimation. Missing at random was assumed for the missing component of the incomplete pairs. Proc mixed procedure in SAS version 9.2 was used for implementation of this analysis.

3. Results and discussion

Regardless of imaging modality, image stabilization is an important consideration during image analysis as motion artifacts decrease the image resolution and the accuracy of image quantification. Figure 8 illustrates vessel annotation with and without the subject stabilization and Fig. 9 compares aggregated images computed with and without subject stabilization. Comparing with the individual frame in Fig. 9(A), both aggregated images (Figs. 9(B) and 9(C)) give better visualization of dim lymphatic vessel structures. However, the vessels are blurred and duplicated in the aggregated image computed without subject stabilization (Fig. 9(B)) preventing accurate mapping of lymph flow (Fig. 9(D)) and hence accurate quantification of lymphatic contractile function. For a sequence of 311 images, an average

#169247 - $15.00 USD Received 24 May 2012; accepted 10 Jun 2012; published 22 Jun 2012

tracking error of 1.04 ± 0.82 pixels was calculated between the results obtained when manually tracking visual landmarks and from the subject stabilization algorithm.

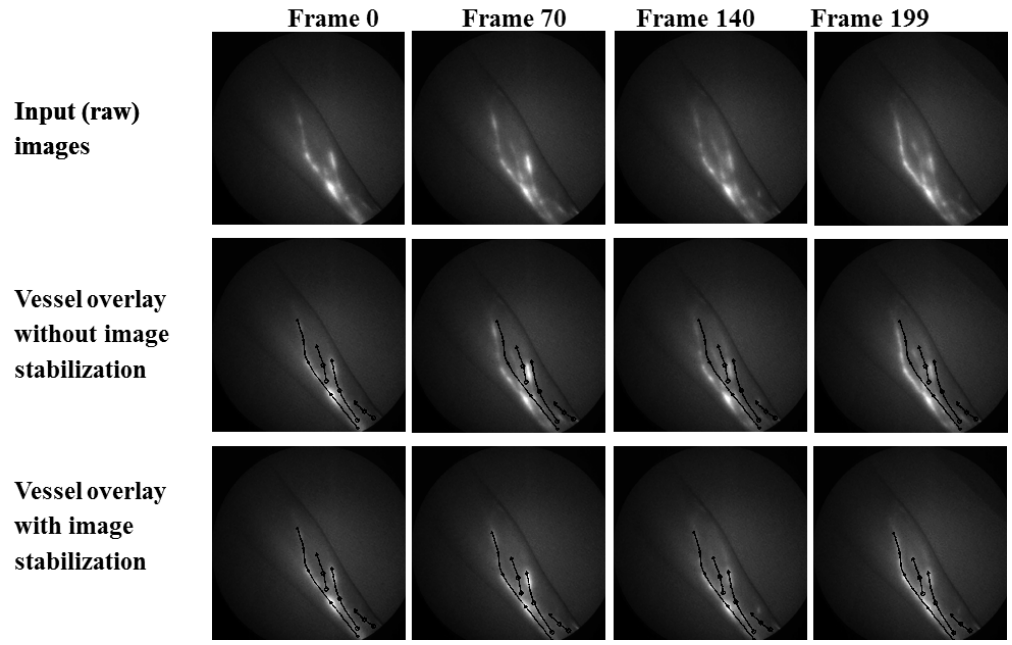

Fig. 8. Images illustrating vessel annotation with (bottom row) and without (middle) subject stabilization.

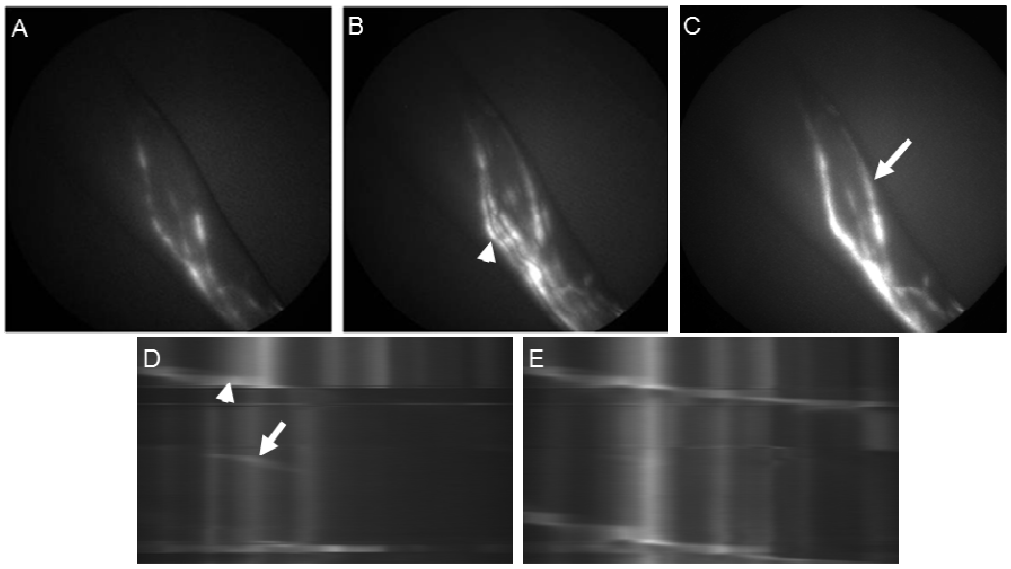

Fig. 9. Vessel enhanced, aggregated images of the lymphatics with (C) and without (B) subject stabilization and the corresponding flow maps (E and D respectively) for the left most vessel. (A) is a snapshot of the lymphatics at a single point in time. (B) Note the appearance of phantom lymphatic vessels (arrowhead) due to motion artifacts in the unstablized aggregated image and (C) the reduction of noise artifact and clear delineation of dim lymphatic vessels (arrow) in the stabilized image as compared to (A). Note also the shortened (arrowhead) flow line and the introduction of an additional flow line (arrow), which corresponds to a neighboring lymphatic vessel, in (D) resulting from subject movement.

#169247 - $15.00 USD Received 24 May 2012; accepted 10 Jun 2012; published 22 Jun 2012

Within the nine subjects analyzed, 820 propulsion events resulting in 820 apparent velocity and 433 period measurements were quantified using manual analysis while 1012 propulsion events, resulting in 1012 apparent velocity and 568 period measurements, were quantified using ALFIA. Because only one propulsion event was often observed in a given sequence of images, fewer period measurements as compared to velocity measurements were obtained. Figure 10 shows plots of the average apparent velocities and periods for each subject obtained manually and from ALFIA. The overall average apparent velocity and standard deviation across all the subjects was 0.9 ± 0.6 cm/s using manual analysis and 0.9 ± 0.5 cm/s using ALFIA while the average periods were 58.1 ± 59.1 s and 64.4 ± 64.0 s respectively. The statistical analysis, which utilized all the individual measurements, confirmed that there was no significant difference between the results from manual analysis and ALFIA with p-values of 0.415 for the apparent velocities and 0.075 for the periods. While no statistically significant difference was observed in the period measurements, a trend was observed with the period calculated with ALFIA being slightly longer than that obtained from manual analysis.

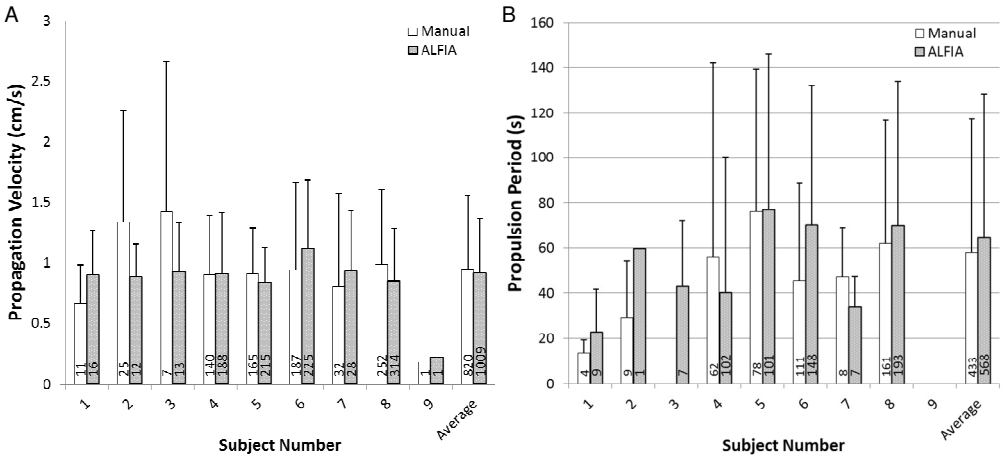

Fig. 10. Plots of the average (A) apparent propagation velocity and (B) propulsion period for each of the nine subjects imaged in this study as well as the overall averages for all participants. The number superimposed on each bar denotes the number of measurements included in each average.

The number of velocity measurements acquired ranged from 1 in one subject using both the manual analysis and ALFIA to 252 and 314 respectively in another subject. Corresponding differences in the numbers of period measurements were also observed. While the number of observed propulsion events varies greatly between subjects, it is not unusual as we have previously shown that in general fewer propulsion events are seen in subjects with lymphatic diseases [7]. In all but two cases, more propulsion events were quantified in each subject using ALFIA, possibly as a result of the vessel stabilization feature implemented in ALFIA as at times subject movement prevented quantification using manual analysis. Additionally, the trend toward increased propulsion period is likely also due to the vessel stabilization feature which allows longer segments and hence more consecutive propulsion events to be quantitated than with manual analysis.

As shown in Fig. 11, the differences in the velocities and periods in the control limbs and the asymptomatic and symptomatic limbs of the subjects with lymphedema were subtle or non-significant due to the high variability in the measurements. However, the numbers of velocity and period measurements were nearly a tenth that seen in the controls and asymptomatic limbs indicative of reduced lymphatic function in disease. Similar results were demonstrated previously by Rasmussen *et al.* in a study of 24 control and 20 unilateral lymphedema subjects [7].

#169247 - $15.00 USD Received 24 May 2012; accepted 10 Jun 2012; published 22 Jun 2012

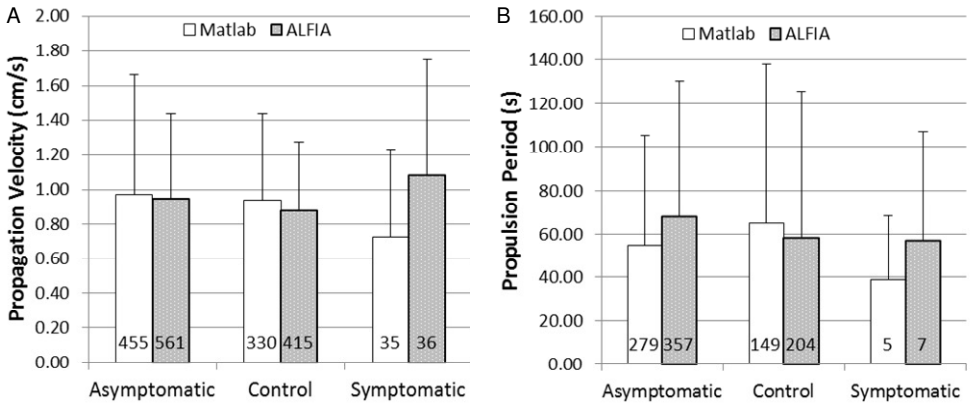

Fig. 11. Plots of the average (A) apparent propagation velocity and (B) propulsion period as a function of limb diagnosis. The number superimposed on each bar denotes the number of measurements included in each average.

While similar algorithms were less effective in the hemovascular system, the nature of NIRF lymphatic imaging and of the lymphatic system itself tend to be more amenable to this type of analysis. Intradermal administration deposits a depot of contrast agent that is gradually taken up by the lymphatic capillaries to form multiple boluses over time, eliminating both the need to inject multiple boluses of contrast agent directly into an artery and the need to time the injections with a set cardiac rhythm. Additionally, the slower lymphatic propagation velocities, as compared to rapid arterial flow velocities of ~50 cm/s in the common carotid artery [19], facilitates bolus tracking over longer timeframes further reducing the need to precisely trigger image capture to ensure visualization of contrast agent at both the beginning and end of the vessel segment of interest. Furthermore, because lymphatic propagation velocity is computed and not the volumetric flow rate, the effect of vessel bifurcation or convergence on the velocity appears to be minimal.

4. Conclusion

In conclusion, we have developed and validated the base algorithms of ALFIA which is designed to facilitate the quantitative analysis of NIRF images for lymphatic contractile function. ALFIA offers several distinct analytic advantages over manual analysis such as image stabilization, improved flow-line identification techniques, and automated computation and exportation of the functional parameters of apparent propagation velocity and propulsion period. With the base algorithms validated, further development of ALFIA into an automated analysis tool will commence. Additional features under development, such as automatic identification of (i) sequential image segments with functional data, (ii) lymphatic vessels, and (iii) flow-lines, will further enhance the utility of the software, significantly decrease required analysis time and user interaction, and may facilitate its translation into the clinic for real-time, quantitative analysis of lymphatic contractile function using NIRF imaging techniques. The ability to visualize and quantify lymphatic function in real-time may in turn provide opportunities to better understand lymphatic disorders, assess the efficacy of lymphatic therapies, and develop personalized lymphatic therapies.

Acknowledgments

The authors thank Kristen E. Adams, Melissa B. Aldrich, Milton V. Marshall, Caroline F. Fife, Erik A. Maus, Latisha A. Smith, and Renie Guilliod for their contributions to this work, including subject imaging and clinical research coordination. This study was sponsored in parts by Tactile Systems Technology, Inc. (Minneapolis, MN), and the National Institutes of Health (R01 HL092923 and U54 CA136404).

#169247 - $15.00 USD Received 24 May 2012; accepted 10 Jun 2012; published 22 Jun 2012